Covalent and Noncovalent Modifications Induce Allosteric Binding Behavior in a Monoclonal Antibody†

Robert C. Blake, II,*,‡ Xia Li,§,|| Haini Yu,§ and Diane A. Blake§

College of Pharmacy, 1 Drexel Drive, Xavier University of Louisiana, New Orleans, Louisiana 70125, Department of Biochemistry, Tulane University Health Sciences Center, 1430 Tulane Avenue, New Orleans, Louisiana 70112, and Beijing Vegetable Research Institute, Beijing, China

Received October 17, 2006; Revised Manuscript Received November 30, 2006

ABSTRACT: Detailed equilibrium binding studies were conducted on a monoclonal antibody (8A11) directed against UO_2^{2+} complexed with 2,9-dicarboxy-1,10-phenanthroline (DCP−UO_2^{2+}). Covalent modification of 8A11 with amine-reactive derivatives of Cy5 or Alexa 488 altered the binding curves obtained with DCP−UO_2^{2+} from hyperbolic to sigmoidal, the latter characterized by Hill coefficients of 1.5−1.6. Binding curves obtained with DCP−UO_2^{2+} and the bivalent $(Fab)_2$ or the monovalent Fab fragments derived from limited proteolysis of the covalently modified 8A11 were characterized by Hill coefficients of 1.2 and 1.0, respectively. Incubation of 8A11 with saturating concentrations of the Fab fragments of goat antibodies directed against the Fc portion of mouse IgG increased the affinity of the native 8A11 for DCP−UO_2^{2+} by 3-fold. Conversely, incubation of the 8A11−Cy5 covalent conjugate with saturating concentrations of protein G (which likewise binds to the constant regions of mouse IgG) decreased the affinity of the primary antibody for DCP−UO_2^{2+} by 4-fold. In addition, the binding curves obtained with 8A11−Cy5 and DCP−UO_2^{2+} species changed from sigmoidal to hyperbolic at high concentrations of protein G. The presence of the antigen had a reciprocal effect on the binding of protein G to the 8A11−Cy5 conjugate; incubation of the 8A11−Cy5 conjugate with saturating concentrations of DCP−UO_2^{2+} decreased the affinity of the conjugate for protein G by 20-fold. These complex binding data were interpreted in terms of a free energy binding model in which (i) 2 mol of DCP−UO_2^{2+} and 1 mol of protein G bind to each mole of the 8A11−Cy5 conjugate, (ii) binding of the first equivalent of DCP−UO_2^{2+} to the antibody promotes the binding of the second equivalent of antigen in the absence of protein G, and (iii) DCP−UO_2^{2+} and protein G oppose each other's binding to the antibody. This is the first detailed description of the energetic balance of reciprocal binding events among the antigen binding sites and distant points on the constant portion of an immunoglobulin.

An earlier report from our laboratories described the extraordinary allosteric binding properties of a monoclonal antibody directed toward an epitope comprised of Pb(II) complexed with a protein conjugate of a common metal ion chelator (*1*). In the presence of certain combinations of chelators and metal ions, this antibody, designated as 5B2, exhibited homotropic allosteric binding behavior, where the binding of the first equivalent of antigen to the divalent antibody increased the affinity for the antigen at the remaining unoccupied antigen binding site. In the presence of other combinations of chelators and metal ions, 5B2 exhibited heterotropic allosteric binding behavior, where the binding of a small molecule to an additional binding site on the antibody other than the antigen binding site served to alter the affinity of the antibody for antigen. To our knowledge, this was the first detailed description of complex allosteric binding behavior in a purified monoclonal antibody.

In contrast to the unexpected binding behavior exhibited by 5B2, all of the monoclonal antibodies directed toward chelated metal ions described previously appeared to bind their antigens or analogs thereof with the usual hyperbolic concentration dependence, where the two antigen binding sites behave identically and independently (*2*−*15*). The most recent of these reports described the isolation and functional characterization of three monoclonal antibodies directed toward chelated uranium(VI) (*15*). Each of these three antibodies, including one designated as 8A11, bound chelated uranyl ions with a normal, hyperbolic concentration dependence and an affinity for the antigen in the low nanomolar to midnanomolar range.

As part of an ongoing effort to develop immunoassays for chelated uranium on both a portable and an in-line flow fluorimeter, antibody 8A11 was fluorescently labeled using two different strategies. When 8A11 was covalently coupled via available lysine residues to either Alexa Fluor 488 or Cy5,[1] two amine-reactive fluorescent dyes, the resulting fluorescent antibody conjugate exhibited homotropic positive cooperativity in its binding interactions with chelated uranium. That is, when one of the two binding sites on the covalently modified 8A11 was occupied with bound antigen, the affinity of the remaining site on the antibody for chelated

† This research was supported by National Institutes of Health Grant GM08008-26S1 (R.C.B.) and the Office of Science (BER) of the U.S. Department of Energy, Grant DE-FG02-98ER62704 (D.A.B.).

* To whom correspondence should be addressed. Phone: (504) 520-7489. Fax: (504) 520-7954. E-mail: rblake@xula.edu.

‡ Xavier University of Louisiana.

§ Tulane University Health Sciences Center.

|| Beijing Vegetable Research Institute.

10.1021/bi062164j CCC: $37.00
Published on Web 01/17/2007

uranium appeared to increase. Proteolytic cleavage of the fluorescently labeled 8A11 to produce the bivalent $(Fab)_2$ fragment yielded an active preparation that bound chelated uranium with a lower degree of positive cooperativity than did the intact antibody. Proteolysis of the intact fluorescent antibody to produce the monovalent Fab fragment yielded a preparation that bound chelated uranium with no evidence of positive cooperativity.

When 8A11 was incubated with fluorescently labeled Fab fragments of goat antibodies directed toward the Fc portion of mouse antibodies, the resulting fluorescent protein complex exhibited a higher affinity for chelated uranium than did the native 8A11 alone. The addition of protein G, a bacterial protein that also binds to the Fc portion of mouse antibodies, to Cy5-modified 8A11 produced a protein complex that exhibited a lower affinity for chelated uranium than did the 8A11−Cy5 conjugate alone. This protein G-dependent decrease in the affinity of the 8A11−Cy5 conjugate for chelated uranium was dose-dependent. Similarly, chelated uranium served to decrease the affinity between the 8A11−Cy5 conjugate and protein G, also in a dose-dependent manner. These reciprocal binding effects between protein G and chelated uranium provided strong evidence that binding to the Fc portion of the intact 8A11 could influence the strength of the interactions at the spatially distant antigen binding sites, and vice versa. The observations reported herein provide new insights into a fundamental property of antibody functional behavior that appears to have been largely unnoticed (*16*).

EXPERIMENTAL PROCEDURES

Materials. Purified 8A11 anti-uranium monoclonal antibody and BSA covalently modified with an isothiocyanate derivative of DCP (BSA-DCP) were available from a previous study (*15*). The succinimidyl ester of the Alexa Fluor 488 carboxylic acid (hereafter termed Alexa 488) and Zenon One Alexa Fluor 647 (hereafter termed Zenon 647) were purchased from Molecular Probes, Inc. (Eugene, OR). The Cy5 Mono-Reactive Dye Pack was obtained from Amersham Biosciences Corp. (Piscataway, NJ). Recombinant protein G that lacked detectable binding to BSA was a product of Sigma Chemical Co. (St. Louis, MO). The horseradish peroxidase and Cy5 conjugates of affinity-purified goat anti-mouse $(Fab)_2$-specific antibodies were obtained from Jackson ImmunoResearch Laboratories, Inc. (West Grove, PA). The ImmunoPure IgG_1 Fab and $(Fab)_2$ Preparation Kit was purchased from Pierce Biotechnology, Inc. (Rockford, IL). 2,9-Dicarboxy-1,10-phenanthroline was obtained from Alfa-Aesar (Wood Hill, MA). The 2,9-dicarboxymethylester-, 2,9-dihydroxymethyl-, and 2,9-diphosphonatomethyl-substituted 1,10-phenanthrolines were available from a previous study (*15*). Uranyl diacetate (ACS-grade) was a product of Mallinckrodt Chemical Works (St. Louis, MO). All other chemicals were reagent grade.

The KinExA 3000 flow fluorimeter and polystyrene beads, 98 μm average diameter, were purchased from Sapidyne Instruments, Inc. (Boise, ID).

Fluorescent Labeling of 8A11. Purified intact 8A11 was covalently modified with either the succinimidyl ester of Alexa 488 carboxylic acid or the monofunctional *N*-hydroxysuccinimidyl ester of Cy5 according to the respective detailed instructions supplied by the manufacturers of each amine-reactive fluorescent dye. The extent of covalent labeling in each case was estimated by spectrophotometric measurements conducted on pooled fractions of the final protein−dye conjugates after removal of excess unconjugated fluorescent dye. The absorption coefficients of Alexa 488, Cy5, and intact mouse IgG were taken to be 71 000 (494 nm), 250 000 (650 nm), and 203 000 (280 nm) M^{-1} cm^{-1}, respectively. The contribution of each fluorescent dye to the absorbance at 280 nm in the conjugated product was subtracted using absorption coefficients for Alexa 488 and Cy5 of 7810 and 12 500 M^{-1} cm^{-1}, respectively, at 280 nm (per the manufacturer's data sheets). The dye/protein ratios determined in this manner were 3.97 and 0.98 for the 8A11 conjugates with Alexa 488 and Cy5, respectively.

Intact 8A11 or the 8A11−Cy5 conjugate was noncovalently labeled by incubation for at least 24 h at 4 °C with sufficient Zenon 647 reagent to achieve a 3/1 molar ratio of labeled goat Fab to intact mouse antibody.

Preparation of Antibody Fragments. Proteolytic fragments of 8A11 covalently modified with Cy5 were prepared using the ImmunoPure IgG_1 Fab and $(Fab)_2$ Preparation Kit from Pierce. Briefly, separate samples of the intact antibody were subjected to limited proteolytic cleavage with immobilized ficin. The activity of the immobilized ficin and the reduction of disulfide bonds in the antibody were purposefully controlled by varying the concentration of cysteine activator as described in the manufacturer's printed instructions. The progress of each proteolytic digestion was assessed by SDS−PAGE followed by Western blotting using light chain-specific antibodies labeled with horseradish peroxidase. The Fab preparation yielded a single band that migrated at approximately 25 000 Da, while the $(Fab)_2$ preparation yielded two bands of approximately equal staining intensities around the same mass of 25 000 Da (data not shown). Undigested IgG_1 and Fc fragments were removed when the reaction products were passed through a column of immobilized protein G. The final total protein yields recovered from the preparations of $(Fab)_2$ and Fab were 13.9 and 61.3%, respectively, of the initial protein present in the intact IgG_1. Both types of purified fragments retained the fluorescence properties of Cy5. If one arbitrarily assumes that the $(Fab)_2$ and Fab fragments have absorption coefficients of 135 000 and 68 000 M^{-1} cm^{-1}, respectively [that is, that aromatic amino acids are distributed more or less equally among the $(Fab)_2$ and Fab portions of the immunoglobulin], then the dye/protein ratios for the $(Fab)_2$ and Fab fragments were determined to be 3.15 and 1.58, respectively.

Equilibrium Binding Studies. Equilibrium measurements on the binding interactions of antibody 8A11 and its

[1] Abbreviations: Cy5, indodicarbocyanine dye; DCP, 2,9-dicarboxy-1,10-phenanthroline; DME, 2,9-dicarboxymethyl ester 1,10-phenanthroline; DHM, 2,9-dihydroxymethyl-1,10-phenanthroline; DPP, 2,9-diphosphonatomethyl-1,10-phenanthroline; Hepes, *N*-(2-hydroxyethyl)-piperazine-*N*′-2-ethanesulfonic acid; HBS, Hepes-buffered saline [137 mM NaCl, 3 mM KCl, and 10 mM Hepes (pH 7.4)]; BSA, bovine serum albumin; SDS−PAGE, sodium dodecyl sulfate−polyacrylamide gel electrophoresis; Fab, fragment antigen binding (monovalent); $(Fab)_2$, fragment antigen binding (bivalent); F_c, fragment crystallizable; 8A11−Alexa 488, antibody 8A11 covalently modified with Alexa Fluor 488; 8A11−Cy5, antibody 8A11 covalently modified with Cy5; 8A11−Zenon 647, antibody 8A11 noncovalently modified with Zenon One Alexa Fluor 647; 8A11−Cy5−Zenon 647, antibody 8A11 covalently modified with Cy5 and noncovalently modified with Zenon One Alexa Fluor 647.

proteolytic fragments were performed using a KinExA 3000 flow fluorimeter. The KinExA 3000 device is an immunoassay instrument that exploits an immobilized form of the antigen to separate and quantify the fraction of unoccupied binding sites that remain in reaction mixtures of antibody and antigen. The increased sensitivity of this flow fluorimeter compared with those of other instrumental methods for studying protein−ligand binding interactions, such as isothermal titration calorimetry, permits one to easily study antibody−antigen interactions with equilibrium dissociation constants in the low nanomolar range. Further, the KinExA assays yield data for binding interactions between soluble partners in a homogeneous solution, unlike other heterogeneous methods that quantify binding reactions with an immobilized reaction partner (*17*−*19*). The general KinExA assay procedures have been described in detail elsewhere (*5*, *20*, *21*).

For experiments that focused on the antigen binding properties of 8A11 and its derivatives, the immobilized capture reagent was comprised of uniform polystyrene beads adsorption-coated with BSA-DCP loaded with UO_2^{2+}. Polystyrene beads (200 mg) were incubated with 1.0 mL of 100 μg/mL BSA-DCP for 1 h at 37 °C. The beads were washed twice with 1.0 mL of HBS, and then any remaining adsorption sites on the beads were blocked by incubation for 1 h at 37 °C with BSA (10 mg/mL in HBS containing 0.03% NaN_3). Beads were stored in this blocking solution for up to 2 months at 4 °C. Immediately before being used, the beads were diluted into 30 mL of HBS amended with 30 μM uranyl diacetate to saturate the immobilized DCP with UO_2^{2+}. The excess uranyl ions were washed away when individual aliquots of the coated beads were packed into the capillary observation cell.

All of the equilibrium measurements described below were conducted at 25 °C in Hepes-buffered saline (HBS), comprised of 137 mM NaCl, 3.0 mM KCl, and 10 mM Hepes (pH 7.4). When the soluble antigen consisted of UO_2^{2+} complexed with DCP, DME, or DHM, all of the binding reaction mixtures contained a constant total concentration of 1.0 μM UO_2^{2+} and different limiting concentrations of the chelator. Previous studies have shown that DCP and its analogues bound with nanomolar affinity to UO_2^{2+} (*15*). The solution conditions employed in these experiments thus dictated that more than 99.6% of the soluble chelator was present as the 1/1 complex with UO_2^{2+}. Control experiments indicated that 1.0 μM UO_2^{2+} alone did not inhibit the binding of 8A11 or any of its derivatives to the immobilized antigen. When the soluble antigen consisted of micromolar concentrations of DPP and UO_2^{2+}, the chelator and the uranyl ions were present at equimolar concentrations.

Quantification of the 8A11−Alexa 488 conjugate captured and retained on the immobilized antigen was accomplished by monitoring the fluorescence of the Alexa 488 dye with the Blue Filter Set (part no. 544125) supplied by Sapidyne. Equilibrium reaction mixtures contained a total 8A11−Alexa 488 concentration of 0.8 nM; in the absence of a soluble antigen, this level of labeled antibody produced a fluorescence signal of >1.5 V with millivolt noise. Quantification of 8A11 labeled with Cy5 or Zenon 647 was accomplished by monitoring the fluorescence of the respective dyes with the Red Filter Set (part no. 544413) supplied by Sapidyne. Equilibrium reaction mixtures of 8A11−Cy5 or each of the two fluorescent proteolytic fragments contained a total protein concentration of 0.2 nM; in the absence of a soluble antigen, this level of labeled protein produced a fluorescence signal of approximately 2.0 V. Equilibrium reaction mixtures of 8A11−Zenon 647 or 8A11−Cy5−Zenon 647 contained a total 8A11 concentration of 0.1 nM.

For experiments that focused on the protein G binding properties of 8A11−Cy5, the immobilized capture reagent was comprised of uniform polystyrene beads adsorption-coated with protein G. Polystyrene beads (200 mg) were incubated with 1.0 mL of 100 μg/mL protein G for 1 h at 37 °C. The beads were washed twice with 1.0 mL of HBS, and then any remaining adsorption sites on the beads were blocked by incubation for 1 h at 37 °C with BSA (10 mg/mL in HBS containing 0.03% NaN_3). The beads were diluted into 30 mL of HBS immediately before being used. The excess BSA was washed away when individual aliquots of the coated beads were packed into the capillary observation cell.

Quantification of 8A11−Cy5 or 8A11−Cy5−Zenon 647 captured and retained by the immobilized protein G was accomplished by monitoring the fluorescence of the labeled antibody with the Red Filter Set. Equilibrium reaction mixtures of 8A11−Cy5 or 8A11−Cy5−Zenon 647 contained a total 8A11 concentration of 0.2 or 0.1 nM, respectively.

RESULTS

Homogeneous versus Synergistic Binding. When the monoclonal anti-uranium antibody designated as 8A11 was covalently modified by reaction with amine-reactive derivatives of either Cy5 or Alexa 488, the resulting highly fluorescent primary antibody appeared to bind chelated uranium in a manner consistent with homotropic positive cooperativity. That is, the covalently modified antibody behaved as though it bound the second molecule of chelated uranium with higher affinity than it bound the first molecule. The assay used to discriminate between this type of synergistic binding and that anticipated for a simple homogeneous binding model is illustrated with the data shown in Figure 1.

Figure 1A shows representative examples of the time courses for the fluorescence signals when different equilibrium reaction mixtures of 8A11−Cy5 and DCP−UO_2^{2+} were assayed on the KinExA. The concentration of the fluorescent antibody was held constant at 0.2 nM, while the concentration of DCP−UO_2^{2+} was varied over a wide range. The fluorescence signal from 0 to 50 s (only a small portion of which is shown in the figure) corresponded to the background signal generated while buffer alone passed through the packed column of microbeads. The beads coated with immobilized DCP−UO_2^{2+} were then exposed to solutions of Cy5-labeled 8A11 antibody equilibrated with different concentrations of soluble DCP−UO_2^{2+} (from 60 to 120 s), followed by a buffer wash to remove any excess unbound antibody (from 120 to 240 s). When the equilibrium mixture contained a saturating concentration of soluble DCP−UO_2^{2+} (curve e), none of the 8A11−Cy5 was available to bind to the immobilized antigen on the beads, and the instrument response corresponded to the fluorescence of 8A11−Cy5 during its transient passage past the beads in the observation cell. The signal failed to

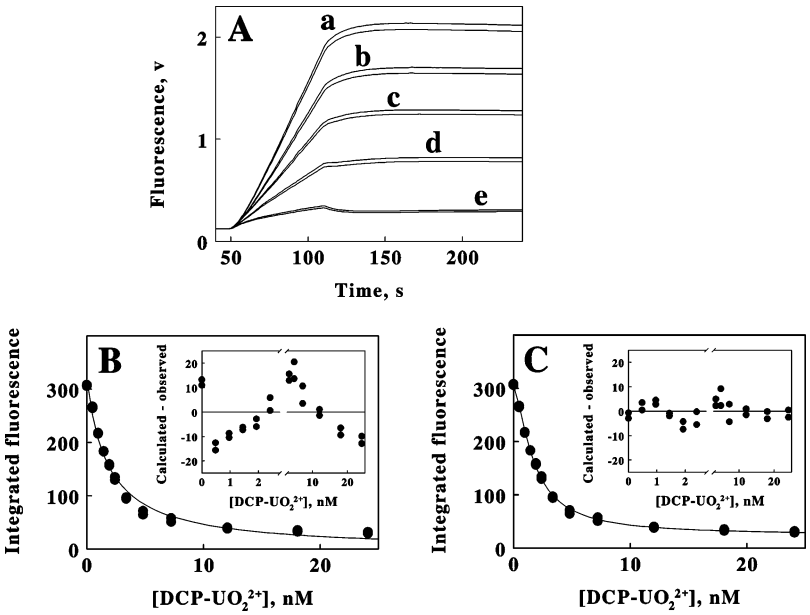

FIGURE 1: Assay for distinguishing between homogeneous and synergistic binding of chelated uranium to monoclonal antibody 8A11 covalently modified with Cy5. (A) Selected time courses of individual fluorescence responses when beads bearing immobilized DCP−UO_2^{2+} were exposed to different equilibrium reaction mixtures of soluble fluorescent antibody and DCP−UO_2^{2+}. Soluble reagent concentrations were as follows: 0.2 nM 8A11−Cy5 and 0, 0.8, 1.9, 3.4, and 100 nM DCP−UO_2^{2+} in curves a−e, respectively. Each assay was performed in duplicate. (B) Secondary plot of the cumulative fluorescence in each assay, consisting of the integrals under the time courses over the interval of 150−240 s, as a function of the concentration of DCP−UO_2^{2+} in the respective reaction mixtures. The hyperbolic curve drawn through the data points was generated from the one-site, homogeneous binding model using a K_d of 1.8 nM. (C) Same binding data as in panel B. The sigmoidal curve drawn through the data points was generated from a multiple-site, synergistic binding model using values for $K_{0.5}$ and the Hill coefficient of 1.7 nM and 1.5, respectively. The insets in panels B and C are residual plots showing the differences among the experimental data and the theoretical data calculated using the homogeneous and synergistic binding models, respectively. All binding assays were conducted in duplicate; in many cases, the error in the determinations was less than the diameter of the data points.

return to that of the background, indicating a very slight level of nonspecific binding to the beads of 8A11−Cy5 saturated with antigen. When soluble DCP−UO_2^{2+} was omitted from the equilibrium mixture (curve a), all of the 8A11−Cy5 antibody was available to bind to the beads, and the instrument response from 60 to 120 s was the sum of two contributions: the fluorescence of the unbound labeled antibody in the interstitial regions among the beads and that of 8A11−Cy5 that was captured by the immobilized antigen on the beads. Binding of 8A11−Cy5 to the immobilized antigen was an ongoing process that produced a positive slope in this portion of the curve. When excess unbound 8A11−Cy5 was removed from the beads, the signal that remained was the sum of that from the nonspecifically bound antibody plus that of 8A11−Cy5 specifically captured by the immobilized antigen on the beads. Equilibrium mixtures that contained soluble DCP−UO_2^{2+} at concentrations intermediate between those of zero and saturation thus provided intermediate instrument responses (curves b−d) from which the concentration of unoccupied (and, by difference, the occupied) antigen binding sites on the anti-uranium antibody in each mixture could be determined.

Figure 1B illustrates the approach taken to obtain the fraction of unoccupied binding sites in 8A11−Cy5 as a function of the total concentration of DCP−UO_2^{2+}. Individual instrument responses were taken from each time course of fluorescence versus time by calculating the integral under each curve from 160 to 240 s. The value of each integral was then plotted as a function of the total concentration of soluble DCP−UO_2^{2+}. The following equation was fit to the data in Figure 1B:

$$I_{exp} = I_0 - (I_0 - I_\infty)[X]/([X] + K_{0.5}) \quad (1)$$

where I represents the integral of each curve over the interval of 160−240 s, the subscripts 0, exp, and ∞ refer to experimental traces corresponding to an antigen concentration of zero, an intermediate antigen concentration, and an infinite antigen concentration, respectively, [X] is the total antigen concentration, and $K_{0.5}$ is the concentration of antigen that resulted in occupancy of half of the antibody's binding sites with antigen. The values of I_0, I_{exp}, and [X] were available from the individual KinExA assays, while the values of I_∞ and $K_{0.5}$ were obtained from the nonlinear regression fit of eq 1 to the data. Equation 1 represents a one-site, homogeneous binding model in which the values of the experimental data decrease hyperbolically to some limiting value as the antigen concentration increases. Homogeneous binding is anticipated for an antibody−antigen interaction where the two antigen binding sites on the antibody behave as though they are equal and independent. The curve drawn through the data points in Figure 1B was generated using eq 1 and the values for I_∞ and $K_{0.5}$ of 3.2 volt-s and 1.8 nM, respectively.

The ability of eq 1 to accurately describe the equilibrium binding data shown in Figure 1B was ascertained by the inspection of residual plots such as the one shown in the inset of Figure 1B. The semilogarithmic residual plot shows the differences among the experimental data and the theoretical curve calculated using eq 1 and values for I_∞ and $K_{0.5}$ as

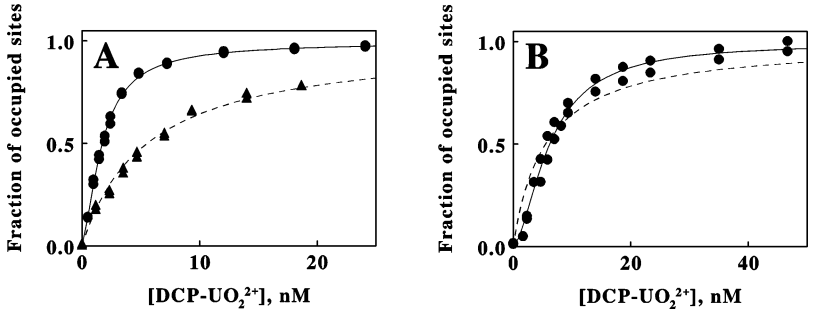

FIGURE 2: Effect of different amine-reactive fluorophores on the antigen binding behavior of antibody 8A11. (A) Comparison of the equilibrium binding of DCP−UO_2^{2+} to native 8A11 (▲) and the covalent conjugate of 8A11 with the *N*-hydroxysuccinimidyl ester of Cy5 (●). The dashed curve was generated from the one-site, homogeneous binding model using a K_d of 5.5 nM. The solid curve was generated from the two-site heterogeneous binding model using values for *K*(X) and *K*(X/X) of 5.4 and 0.54 nM, respectively. (B) Comparison of the equilibrium binding of DCP−UO_2^{2+} to native 8A11 (- - -) and the covalent conjugate of 8A11 with the succinimidyl ester of Alexa 488 (●). The data points were omitted from the native 8A11 binding curve for clarity of presentation. The solid curve was generated from the two-site heterogeneous binding model using values for *K*(X) and *K*(X/X) of 30 and 1.3 nM, respectively.

described above. The fraction of occupied binding sites observed below 2.0 nM and above 12 nM DCP−UO_2^{2+} was consistently greater than that predicted theoretically, while the same fraction observed between 2.0 and 12 nM was consistently less than that predicted theoretically. The systematic deviation of long stretches of the experimental data from the calculated curve indicated that there was a poor fit of the data to the homogeneous binding model. When the data for underivatized 8A11 were fit to the same homogeneous binding model, this systematic deviation was not observed (*15*). Thus, this model did not adequately fit all of the data obtained with the 8A11−Cy5 conjugate, in spite of the fact that individual deviations were less than 10%.

Figure 1C shows the slightly sigmoidal curve obtained when the following equation was fit to the binding data from Figure 1B:

$$I_{exp} = I_0 - (I_0 - I_\infty)[X]^n/([X]^n + K_{0.5}{}^n) \quad (2)$$

where *n*, the Hill coefficient, was a number greater than 1.0 and all other terms were the same as those defined for eq 1. Equation 2 represents a multiple-site, synergistic binding model anticipated for a divalent antibody that binds its two antigens with homotropic positive cooperativity. Values for $K_{0.5}$ and *n* of 1.7 nM and 1.5, respectively, were obtained from an iterative nonlinear regression analysis of the binding data according to eq 2. The semilogarithmic plot in the inset of Figure 1C shows the differences among the experimental data and the theoretical curve calculated using eq 2 and the values for $K_{0.5}$ and the Hill coefficient as described above. The random dispersion of the experimental data around the theoretical line was taken as evidence that eq 2 constituted an acceptable model for the binding of DCP−UO_2^{2+} to 8A11−Cy5.

Residual plots such as those described for the data in Figure 1 were constructed and analyzed for every antibody−antigen binding interaction presented herein.

Binding to a Covalently Modified Antibody. Previous studies on the binding of 8A11 and selected congeners of DCP in the presence of UO_2^{2+} demonstrated that the native antibody bound its soluble antigen in a manner consistent with the one-site, homogeneous binding model represented by eq 1 (*15*). In contrast, 8A11 covalently modified with amine-reactive derivatives of Cy5 or Alexa 488 bound the same DCP−UO_2^{2+} complexes in a manner consistent with the multiple-site, synergistic binding model represented by eq 2. In subsequent experiments, the fraction of occupied binding sites on the antibody was calculated as the ratio $(I_0 - I_{exp})/(I_0 - I_\infty)$, which served to normalize the raw fluorescence data and reduce the mathematical expressions for the homogeneous and synergistic binding models to eqs 3 and 4, respectively:

$$\text{fraction of occupied sites} = [X]/([X] + K_d) \quad (3)$$

$$\text{fraction of occupied sites} = [X]^n/([X]^n + K_{0.5}{}^n) \quad (4)$$

where K_d is the equilibrium dissociation constant and $K_{0.5}$ is the concentration of antigen that resulted in occupancy of half of the antibody's binding sites with antigen.

The dashed curves in panels A and B of Figure 2 represent the one-site, homogeneous binding of DCP−UO_2^{2+} to native 8A11 with a K_d of 5.5 nM (*15*). The circles and solid curves in panels A and B of Figure 2 represent the synergistic binding of DCP−UO_2^{2+} to 8A11−Cy5 and 8A11−Alexa 488, respectively. In addition to changing the concentration dependence of antigen binding from hyperbolic to sigmoidal, covalent modification of 8A11 with Cy5 also served to increase the affinity of the antibody for its antigen. Conversely, covalent modification of 8A11 with Alexa 488 had very little effect on the antibody's average affinity for its antigen, although the chemically modified antibody still bound its antigen in a synergistic manner.

While the Hill equation provided an acceptable means of screening the raw fluorescence binding data for evidence of synergistic binding behavior, further interpretation of the binding data was accomplished by adopting the formalism introduced more than a quarter of a century ago by Weber and associates to describe the energetics of multiple-ligand binding to proteins (*22*−*24*). The free energy scheme presented in Figure 3 summarizes the possible energetic interactions between the binding of 2 mol of antigen X to a bivalent antibody P. Each horizontal line in Figure 3 represents the sum of the chemical potentials for the various antibody and antigen species associated with each line. Each vertical arrow represents the free energy change attendant

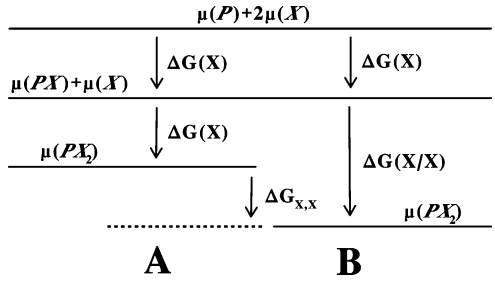

FIGURE 3: Schematic free energy diagram for the independent (A) or synergistic (B) binding of 2 mol of antigen (X) to a bivalent antibody (P). The different chemical species possible in the binding mixture are shown in italics. Each horizontal line represents the overall chemical potential of a particular mixture of free antibody (P), free antigen (X), and antibody−antigen complexes (PX and PX_2); $\mu(i)$ represents the chemical potential of the *i*th species. Each vertical arrow represents the free energy change associated with the changes in the chemical potential due to the binding of the antigen to the antibody. (A) Homogeneous binding where the unconditional free energy changes, $\Delta G(X)$, for the binding of the first and second equivalents of antigen to the antibody are identical. (B) Synergistic binding where the conditional free energy change, $\Delta G(X/X)$, for the binding of the second equivalent of antigen to the antibody is greater (more negative) than the unconditional free energy change for the binding of the first equivalent of antigen to the antibody with no bound antigen. $\Delta G_{X,X}$, the coupling free energy change, is the difference between the conditional and unconditional free energy changes.

with the conversion of one protein complex into another. Column A in Figure 3 describes a situation in which the bivalent protein binds 2 mol of X with equal affinity in energetically independent events. That is, the binding of a second equivalent of X is unaffected by the ligand occupancy at the other binding site for X on the protein. The free energy change, $\Delta G(X)$, that describes the independent binding of either equivalent of X to the protein is defined as an unconditional free energy of binding (*22*−*24*). Column B in Figure 3 describes a situation in which the binding of the first equivalent of X serves to increase the protein's affinity for the second equivalent of X, constituting a working definition of homotropic positive cooperativity. The quantity $\Delta G(X/X)$, defined as a conditional free energy of binding, represents the free energy for the binding of X when 1 equiv of X is already bound to the protein. In the case of homotropic positive cooperativity depicted in column B, the absolute value of $\Delta G(X/X)$ is greater than that of $\Delta G(X)$. The quantity $\Delta G_{X,X}$, defined as the coupling free energy, is the difference between the unconditional and the conditional free energies of binding of X to the protein; $\Delta G_{X,X}$ will necessarily be a negative value if X binds to P with positive cooperativity.

It is evident that the values of $\Delta G(X)$, $\Delta G(X/X)$, and $\Delta G_{X,X}$ are necessary and sufficient to completely describe the energetics of the binding of 2 mol of antigen to 1 mol of antibody, regardless of the nature of the interaction between the two binding sites for X on the protein. Values for all three free energy changes were obtained from the equilibrium binding data presented in panels A and B of Figure 2. Applying the principles of mass action and the conservation of free energy to the binding scheme depicted in Figure 3, we find the saturation function for X to be as follows (*24*):

$$\text{fraction of sites occupied with X} = \frac{[X]/K(X) + [X]^2/K(X)K(X/X)}{1 + 2[X]/K(X) + [X]^2/K(X)K(X/X)} \quad (5)$$

where $K(X)$ and $K(X/X)$ equal $[P][X]/[PX]$ and $[PX][X]/[PX_2]$, respectively. Values for $K(X)$ and $K(X/X)$ of 5.4×10^{-9} and 5.4×10^{-10} M, respectively, were obtained from a nonlinear regression fit of eq 5 to the data in Figure 2A. Substitution of the values of these equilibrium dissociation constants into the relationship $\Delta G = -RT \ln(K_{eq})$ yielded the corresponding values for $\Delta G(X)$ and $\Delta G(X/X)$ of −11.2 and −12.6 kcal/mol, respectively. The corresponding value of $\Delta G_{X,X}$ was calculated as the difference $\Delta G(X/X) - \Delta G(X)$, or −1.4 kcal/mol. Values for $\Delta G(X)$, $\Delta G(X/X)$, and $\Delta G_{X,X}$ of −10.2, −12.1, and −1.9 kcal/mol, respectively, were determined in a fashion analogous to that for the data in Figure 2B. The solid curves drawn through the data points in panels A and B of Figure 2 were generated using eq 5 and the values for the respective equilibrium dissociation constants determined from the nonlinear regression fits.

The thermodynamic analyses summarized above were applied to equilibrium binding studies conducted on the eight possible combinations of four congeners of chelated uranium and two types of covalently modified 8A11 antibodies. Each combination exhibited equilibrium binding behavior consistent with positive homotropic cooperativity; the binding data obtained with all eight antibody−antigen pairs are summarized in Table 1. Equilibrium data obtained previously (*15*) for the nonsynergistic binding of chelated uranium to native, unmodified 8A11 are also included in Table 1. In general, covalent modification of 8A11 created an antibody that (i) bound the first equivalent of antigen with an affinity within ∼2-fold of that of the native 8A11 but (ii) bound the second equivalent of antigen with an affinity 4−20-fold higher than that of the native protein.

Table 1S of the Supporting Information summarizes the equilibrium dissociation constants that were obtained from binding studies conducted with chemically modified 8A11 and each of three different metal-free chelators. In the absence of uranium, covalently modified 8A11 bound each of the metal-free chelators in a simple manner consistent with the one-site, homogeneous binding model; there was no evidence of synergistic antigen binding in any case. Covalent modification of 8A11 with Cy5 or Alexa 488 served to increase or decrease, respectively, the affinity of the antibody for the metal-free chelator relative to the affinity for the same compounds exhibited by the native, unmodified protein without inducing homotrophic positive cooperativity.

Binding to Proteolytic Fragments. It was of interest to determine what effects proteolytic cleavage of the covalently modified 8A11 would have on the unexpected observation that the modified antibody exhibited homotropic positive cooperativity in its binding interactions with chelated uranium complexes. Accordingly, the $(Fab)_2$ and Fab fragments of 8A11−Cy5 were prepared and subjected to the same equilibrium binding studies as those summarized above for the intact antibody.

Figure 4A shows the equilibrium binding data obtained for the interaction of DCP−UO_2^{2+} with the $(Fab)_2$ fragment of 8A11−Cy5. The solid curve drawn through the data points was generated using eq 5 and values for $K(X)$ and $K(X/X)$

Table 1: Equilibrium Binding of Chelated Uranium to Native Antibody 8A11 and 8A11 Covalently Modified with Amine-Reactive Derivatives of Cy5 and Alexa 488

binding partner	K(X) (M)[a]	K(X/X) (M)[a]	$\Delta G_{X,X}$[b] (kcal/mol)
8A11−Cy5			
DCP−UO_2^{2+}	$(5.4 \pm 0.5) \times 10^{-9}$	$(5.4 \pm 0.4) \times 10^{-10}$	−1.4
DME−UO_2^{2+}	$(5.0 \pm 0.4) \times 10^{-9}$	$(5.3 \pm 0.5) \times 10^{-10}$	−1.3
DHM−UO_2^{2+}	$(9.2 \pm 1.1) \times 10^{-8}$	$(1.8 \pm 0.2) \times 10^{-8}$	−1.0
DPP−UO_2^{2+}	$(3.7 \pm 0.4) \times 10^{-6}$	$(1.0 \pm 0.1) \times 10^{-6}$	−0.8
8A11−Alexa 488			
DCP−UO_2^{2+}	$(3.0 \pm 0.9) \times 10^{-8}$	$(1.3 \pm 0.4) \times 10^{-9}$	−1.9
DME−UO_2^{2+}	$(8.5 \pm 0.6) \times 10^{-9}$	$(1.9 \pm 0.1) \times 10^{-9}$	−0.9
DHM−UO_2^{2+}	$(5.7 \pm 1.1) \times 10^{-8}$	$(2.7 \pm 0.4) \times 10^{-8}$	−0.4
DPP−UO_2^{2+}	$(3.8 \pm 0.2) \times 10^{-6}$	$(1.7 \pm 0.1) \times 10^{-6}$	−0.5
native 8A11[c]			
DCP−UO_2^{2+}	$(5.5 \pm 0.2) \times 10^{-9}$		
DME−UO_2^{2+}	$(1.2 \pm 0.1) \times 10^{-8}$		
DHM−UO_2^{2+}	$(8.6 \pm 0.3) \times 10^{-8}$		
DPP−UO_2^{2+}	$(8.7 \pm 0.6) \times 10^{-6}$		

[a] K(X) and K(X/X) are the equilibrium dissociation constants for the synergistic binding of the first and second equivalents of antigen, respectively, to the bivalent antibody. Each value in this table represents binding data obtained from duplicate experiments conducted with 10−12 different concentrations of antigen that spanned from 10 to 90% of the saturation curve. [b] $\Delta G_{X,X}$ is the coupling free energy change for the synergistic binding of 2 equiv of antigen to the bivalent antibody. [c] Values for the equilibrium dissociation constants for the homogeneous binding of chelated uranium to native 8A11 were taken from ref *15*.

of 3.3 and 1.1 nM, respectively. The inset in Figure 4A is a semilogarithmic residual plot that shows the differences among the experimental data and the theoretical curve calculated using eq 5. The random dispersion of the experimental data around the theoretical line indicated that eq 5 provided an acceptable mathematical description of the binding of DCP−UO_2^{2+} to the $(Fab)_2$ fragment of 8A11−Cy5. A similar analysis of the data in Figure 4A using eq 3, which represents the one-site, homogeneous binding model, generated a residual plot that resembled that shown in Figure 1B (data not shown). Like intact 8A11−Cy5, the corresponding bivalent $(Fab)_2$ fragment appeared to bind DCP−UO_2^{2+} with homotropic positive cooperativity, although the coupling free energy for the $(Fab)_2$ fragment was −0.7 kcal/mol, significantly lower than the value of −1.4 kcal/mol obtained with the intact antibody.

Analyses of the binding interactions of the $(Fab)_2$ fragment with the uranyl complexes of DME, DHM, and DPP revealed that eq 5 also provided the best description for each of these binding interactions as well (primary data not shown). Equilibrium data for the binding of the uranyl complexes of DCP and its congeners to the $(Fab)_2$ fragment of the 8A11−Cy5 conjugate are summarized in Table 2. In all cases, the absolute value of the coupling free energy for the interaction of the $(Fab)_2$ fragment with chelated uranium was less than the coupling free energy of intact 8A11−Cy5 with the same compound, indicating that proteolytic cleavage of the chemically modified antibody served to lower the degree of homotropic positive cooperativity. Proteolytic cleavage of 8A11−Cy5 to its $(Fab)_2$ fragment did not, however, have an appreciable effect on the affinity of the antibody for chelated uranium. Although the values of K(X) and K(X/X) obtained with the $(Fab)_2$ fragment and four DCP−UO_2^{2+} congeners differed slightly from those obtained with intact 8A11−Cy5, no significant trends were evident.

Similar analyses of the binding interactions of the $(Fab)_2$ fragment with metal-free DCP, DME, and DHM revealed that these interactions conformed to the one-site, homogeneous binding model represented by eq 3 (primary data not shown). Values for the equilibrium dissociation constants obtained for each of these three binding interactions are summarized in Table 2S of the Supporting Information.

Figure 4B shows the equilibrium binding data obtained for the interaction of DCP−UO_2^{2+} with the Fab fragment of 8A11−Cy5. The solid curve drawn through the data points was generated using eq 3 and a value for K_d of 1.78 nM. The inset in Figure 4B is a semilogarithmic residual plot that shows the differences among the experimental data and the theoretical curve calculated using eq 3. The random dispersion of the experimental data around the theoretical line indicated that the homogeneous binding model provided an acceptable mathematical description for the binding of DCP−UO_2^{2+} to the Fab fragment of 8A11−Cy5. The data in Figure 4B are representative of those obtained with the Fab fragment and other antigen analogues; the values of K_d extracted from these equilibrium binding studies conducted with either chelator−uranium complexes or metal-free chelators are summarized in Table 2 and Table 2S of the Supporting Information, respectively. Proteolytic cleavage of 8A11−Cy5 to its Fab fragment did not have an appreciable effect on the affinity of the protein for chelated uranium or the metal-free chelators.

Binding to a Noncovalently Modified Antibody. Intact 8A11 was also converted into a highly fluorescent binding reagent by noncovalent modification with Zenon 647. Zenon reagents are the Fab fragments of goat polyclonal antibodies that bind specifically to the Fc portion of mouse antibodies. Zenon 647 comprises goat anti-Fc Fab fragments that are covalently modified with Alexa 647, a fluorescent dye with absorbance and fluorescence properties similar to those of Cy5. Since the fluorescent Zenon reagents are Fab fragments and thus monovalent, they can be used to noncovalently modify primary mouse antibodies without the complications of protein cross-linking and subsequent precipitation that might be observed with the corresponding intact bivalent goat anti-Fc antibodies.

When intact 8A11 was incubated with Zenon 647 directed against the Fc portion of mouse IgG_1, the resulting highly fluorescent noncovalent protein complex bound to chelated uranium with a greater affinity than did the intact 8A11 alone. Figure 5A shows equilibrium binding data for the interaction of DCP−UO_2^{2+} with 8A11 before (curve a) and after (curve b) incubation of the antibody with Zenon 647. Native 8A11 bound DCP−UO_2^{2+} in a homogeneous fashion with a K_d of 5.5 nM (*15*). The fluorescent 8A11−Zenon 647 complex bound to DCP−UO_2^{2+} in a homogeneous fashion with a K_d of 1.5 nM, a 3.6-fold increase in affinity. Table 3 includes the values of K_d obtained when the 8A11−Zenon 647 complex was incubated with different concentrations of seven different antigen analogues. Each of the equilibrium binding curves obtained with these seven combinations of chelator and uranium showed homogeneous binding with no positive cooperativity (primary data not shown). In each case, the 8A11−Zenon 647 complex bound with higher affinity to the ligand than did the intact 8A11 in the absence of Zenon 647. The observed increases in affinity upon noncovalent

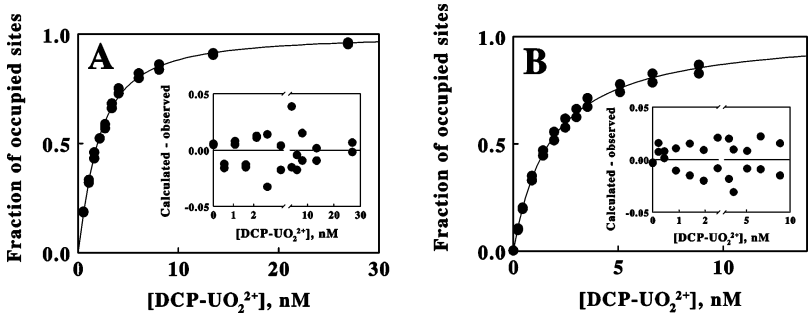

FIGURE 4: Equilibrium binding of chelated uranium to the $(Fab)_2$ and Fab fragments obtained from the proteolysis of the 8A11−Cy5 covalent conjugate. (A) Binding of DCP−UO_2^{2+} to the $(Fab)_2$ fragment. The curve drawn through the data points was generated using the two-site heterogeneous binding model and values for K(X) and K(X/X) of 3.3 and 1.1 nM, respectively. The inset is a residual plot showing the differences among the experimental data from panel A and the theoretical data calculated using the two-site model. (B) Binding of DCP−UO_2^{2+} to the Fab fragment. The curve drawn through the data points was generated using the one-site, homogeneous binding model and a value for K_d of 1.8 nM. The inset is a residual plot showing the differences among the experimental data from panel B and the theoretical data calculated using the homogeneous model.

Table 2: Equilibrium Binding of Chelated Uranium to the $(Fab)_2$ and Fab Fragments Derived from the Proteolysis of the 8A11−Cy5 Covalent Conjugate

	$(Fab)_2$ fragment			Fab fragment
antigen	K(X) (M)[a]	K(X/X) (M)[a]	$\Delta G_{X,X}$[b] (kcal/mol)	K_d (M)[c]
DCP−UO_2^{2+}	$(3.3 \pm 0.2) \times 10^{-9}$	$(1.1 \pm 0.1) \times 10^{-9}$	−0.7	$(1.8 \pm 0.1) \times 10^{-9}$
DME−UO_2^{2+}	$(2.7 \pm 0.2) \times 10^{-9}$	$(1.2 \pm 0.1) \times 10^{-9}$	−0.5	$(1.5 \pm 0.1) \times 10^{-9}$
DHM−UO_2^{2+}	$(1.0 \pm 0.1) \times 10^{-7}$	$(4.1 \pm 0.2) \times 10^{-8}$	−0.5	$(3.4 \pm 0.2) \times 10^{-8}$
DPP−UO_2^{2+}	$(2.0 \pm 0.1) \times 10^{-6}$	$(1.1 \pm 0.1) \times 10^{-6}$	−0.4	$(2.0 \pm 0.1) \times 10^{-6}$

[a] K(X) and K(X/X) are the equilibrium dissociation constants for the synergistic binding of the first and second equivalents of antigen, respectively, to the bivalent antibody. Each value in this table represents binding data obtained from duplicate experiments conducted with 10−12 different concentrations of antigen that spanned from 10 to 90% of the saturation curve. [b] $\Delta G_{X,X}$ is the coupling free energy change for the synergistic binding of 2 equiv of antigen to the bivalent antibody. [c] K_d is the equilibrium dissociation constant for the homogeneous binding of antigen to the monovalent Fab fragment.

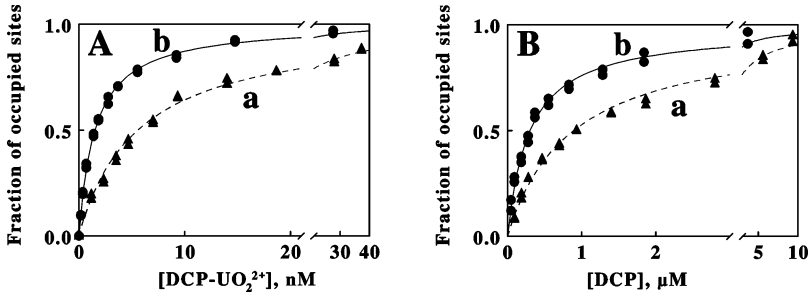

FIGURE 5: Equilibrium binding of chelated uranium and metal-free chelators to 8A11 noncovalently modified with Zenon 647. (A) Binding of DCP−UO_2^{2+} to 8A11 before (a) and after (b) incubation of the antibody with Zenon 647. (B) Binding of metal-free DCP to 8A11 before (a) and after (b) incubation of the antibody with Zenon 647. The curves drawn through the data points in both panels were generated using the one-site, homogeneous binding model and values for the respective K_ds given in Table 3.

modification of 8A11 with Zenon 647 ranged from 3- to 13-fold (shown in parentheses in Table 3).

Since both covalent and noncovalent modifications of 8A11 served to increase the affinity of the mouse antibody for each of seven different antigen analogues, it was of interest to determine whether these effects were additive or mutually exclusive. Accordingly, equilibrium binding studies were conducted on the complex formed when 8A11−Cy5 was incubated with Zenon 647. Figure 5B shows binding data for the interaction of metal-free DCP with 8A11−Cy5 before (curve a) and after (curve b) incubation of the covalently modified antibody with Zenon 647. In the absence of Zenon 647, metal-free DCP bound to 8A11−Cy5 in a homogeneous fashion with an apparent K_d of 3.7×10^{-6} M (Table 1S of the Supporting Information). In the presence of Zenon 647, the binding of DCP to the 8A11−Cy5−Zenon

Table 3: Equilibrium Binding of Chelators and Chelated Uranium to Native 8A11 and the 8A11−Cy5 Covalent Conjugate, Both Noncovalently Modified with Zenon 647

antigen	8A11−Zenon 647 K_d (M)	8A11−Cy5−Zenon 647 K_d (M)
DCP−UO_2^{2+}	$(1.5 \pm 0.1) \times 10^{-9}$ (3.7)[a]	$(1.4 \pm 0.1) \times 10^{-9}$ (2.1)[b]
DME−UO_2^{2+}	$(1.4 \pm 0.1) \times 10^{-9}$ (8.6)	$(1.1 \pm 0.1) \times 10^{-9}$ (2.5)
DHM−UO_2^{2+}	$(2.5 \pm 0.1) \times 10^{-8}$ (3.4)	$(2.4 \pm 0.1) \times 10^{-8}$ (2.3)
DPP−UO_2^{2+}	$(1.4 \pm 0.4) \times 10^{-6}$ (6.5)	$(1.3 \pm 0.1) \times 10^{-6}$ (1.8)
DCP, metal-free	$(4.4 \pm 0.2) \times 10^{-7}$ (8.4)	$(3.4 \pm 0.3) \times 10^{-7}$ (2.6)
DME, metal-free	$(3.3 \pm 0.2) \times 10^{-7}$ (13)	$(2.8 \pm 0.3) \times 10^{-8}$ (53)
DHM, metal-free	$(2.0 \pm 0.1) \times 10^{-5}$ (3.4)	$(1.4 \pm 0.1) \times 10^{-5}$ (1.2)

[a] The number in parentheses in this column is the ratio of the K_d obtained with the native 8A11 divided by the K_d given in the table. [b] The number in parentheses in this column is the ratio of the $K_{0.5}$ obtained with the 8A11 covalently modified with Cy5 divided by the K_d given in the table.

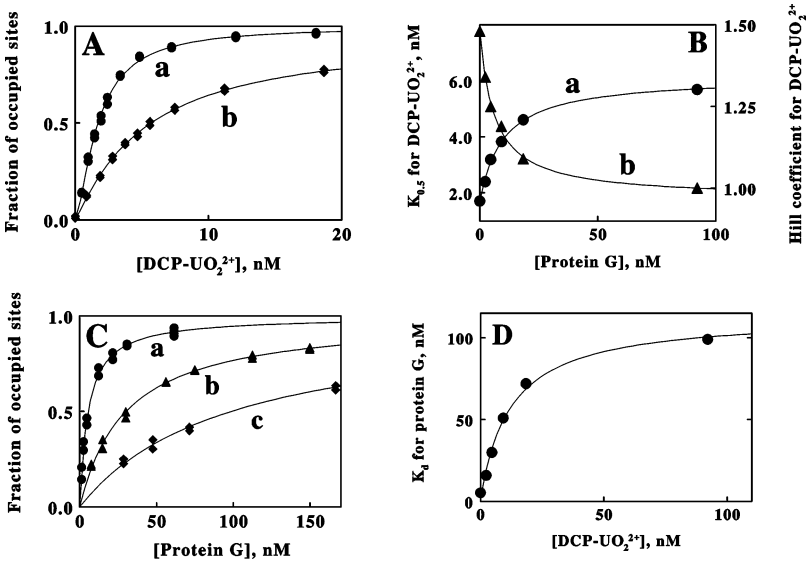

FIGURE 6: Equilibrium binding of DCP−UO_2^{2+} to 8A11 noncovalently modified with protein G. (A) Equilibrium binding of DCP−UO_2^{2+} to 8A11−Cy5 in the presence of 0 (a) and 92 nM protein G (b). The curves drawn through the data points were generated using the multiple-site, synergistic binding model and the following respective values for $K_{0.5}$ and the Hill coefficient: (a) 1.7 nM and 1.5 and (b) 5.7 nM and 1.0, respectively. (B) Dependence of the values of $K_{0.5}$ (a) and the Hill coefficient (b) for the binding of DCP−UO_2^{2+} to 8A11−Cy5 on the concentration of protein G. (C) Equilibrium binding of protein G to 8A11−Cy5 in the presence of 0 (a), 4.6 (b), and 92 nM DCP−UO_2^{2+} (c). The curves drawn through the data points were generated using the one-site, homogeneous binding model and values for K_d of 5.4, 30, and 99 nM for traces a−c, respectively. (D) Dependence of the value of K_d for the binding of protein G to 8A11−Cy5 on the concentration of DCP−UO_2^{2+}.

647 complex conformed to the simple homogeneous curve described by eq 3 with a value for K_d of 3.4×10^{-7} M. Similar results were obtained from binding studies conducted on each of six other antigens (primary data not shown). Regardless of the identity of the antigen, it bound to the 8A11−Cy5−Zenon 647 complex in a simple homogeneous manner; corresponding values of K_d obtained from these seven equilibrium studies are also summarized in Table 3. In each case, the value of K_d obtained with the 8A11−Cy5−Zenon 647 complex was smaller than that obtained with 8A11−Cy5 in the absence of Zenon 647. It was evident that the form of 8A11 that exhibited the greatest affinity for chelated uranium was both covalently and noncovalently modified with Cy5 and Zenon 647, respectively. Control experiments showed that incubation of the $(Fab)_2$ or Fab fragments of 8A11−Cy5, each of which lacked the Fc portion of the intact antibody, with Zenon 647 had no detectable effects on the antigen binding activities of either proteolytic fragment (primary data not shown).

Since Zenon 647 is specific for just the Fc portion of the intact 8A11 or 8A11−Cy5 antibodies, then the Zenon reagents must necessarily bind to the Fc portion and favor an average conformation of the primary antibody that alters the distant antigen binding site(s) in a way that increases the apparent affinity for antigens (a working definition of heterotropic positive cooperativity). Because the binding of Zenon 647 to the Fc portion appeared to increase the affinity of the antibody for the antigen, it was of interest to determine whether the binding of the antigen showed the reciprocal effect of increasing the affinity of the Fc portion for Zenon 647. Unfortunately, the heterogeneous nature of the Zenon 647 reagent (derived from a polyclonal anti-Fc population) discouraged direct binding experiments that characterized the interaction between 8A11−Cy5 and Zenon 647. Instead, a search to identify a homogeneous reagent that would bind to the Fc portion of 8A11 and also affect the activity at the distant antigen binding site was conducted.

Protein G is a bacterial cell wall protein isolated from group G streptococci that binds to mammalian immunoglobulins primarily through their Fc regions (*25*). When intact 8A11−Cy5 was incubated with a constant concentration of protein G, the affinity of the chemically modified antibody for DCP−UO_2^{2+} appeared to decrease, as illustrated in Figure 6A. Curve a in Figure 6A represents the equilibrium binding of DCP−UO_2^{2+} to 8A11−Cy5 in the absence of protein G. Curve a conforms to eq 4 with values for $K_{0.5}$ and the Hill coefficient of 1.71 nM and 1.48, respectively. Curve b represents the binding of DCP−UO_2^{2+} to 8A11−Cy5 in the presence of 92 nM protein G. Curve b conforms to eq 3 with no evidence of homotropic positive cooperativity in the binding of DCP−UO_2^{2+} to 8A11−Cy5; the corresponding value of K_d (or $K_{0.5}$, which is synonymous in this case with K_d) increased from 1.71 to 5.7 nM.

The circles in Figure 6B show the dependence of the values of $K_{0.5}$ for the binding of DCP−UO_2^{2+} to 8A11−Cy5 on the concentration of protein G. The value of $K_{0.5}$ for the binding of DCP−UO_2^{2+} to 8A11−Cy5 increased to a maximum value of 6.2 nM in the presence of an extrapolated infinite concentration of protein G. The triangles in Figure 6B show the dependence of the values of the Hill coefficient for the binding of DCP−UO_2^{2+} to 8A11−Cy5 on the concentration of protein G. As the concentration of protein G increased, the highly cooperative nature of the binding of DCP−UO_2^{2+} to 8A11−Cy5 decreased until the binding curve with the chelated uranium was indistinguishable from that anticipated for a simple, homogeneous binding to a single class of binding sites.

The effect of DCP−UO_2^{2+} on the affinity of the antibody for protein G is illustrated by the binding curves presented in Figure 6C. Curve a in Figure 6C represents the equilibrium

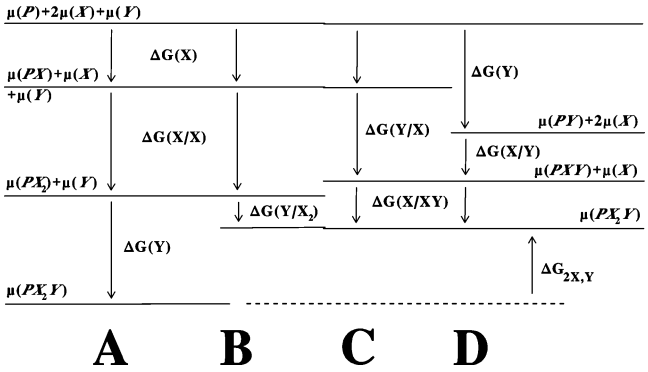

FIGURE 7: Schematic free energy diagram for the binding of 2 equiv of antigen (X) and 1 equiv of a different ligand (Y) to spatially separate sites on an antibody (P). The different chemical species possible in the binding mixture are shown in italics. The horizontal lines and vertical arrows are defined in the legend of Figure 3. (A) X and Y bind independently, but 2 equiv of *X* binds with positive cooperativity. The other three columns represent three different orders of ligand binding where X and Y oppose each other's binding. (B) Two equivalents of X binds with positive cooperativity in the absence of bound Y; Y binds after both equivalents of X. (C) X binds first, followed sequentially by Y and the second equivalent of X. (D) Y binds first, followed by the equal and independent binding of 2 equiv of X.

binding of protein G to 8A11−Cy5 in the absence of DCP−UO_2^{2+}. Protein G bound to 8A11−Cy5 in a homogeneous fashion, with a value for K_d of 5.4 nM. Curves b and c represent the binding of protein G to 8A11−Cy5 in the presence of 4.6 and 92 nM DCP−UO_2^{2+}, respectively. As the concentration of DCP−UO_2^{2+} increased, the affinity of 8A11−Cy5 for protein G decreased. Figure 6D shows the dependence of the values of K_d for the binding of protein G to 8A11−Cy5 on the concentration of DCP−UO_2^{2+}. The affinity of 8A11−Cy5 for protein G decreased 20-fold (extrapolated K_d of 1.1×10^{-7} M) in the presence of an extrapolated infinite concentration of DCP−UO_2^{2+}.

The free energy scheme presented in Figure 7 gives an overview of the energetic interactions that could occur among ligands X and Y with a protein P that is capable of binding 2 mol of X and 1 mol of Y at spatially different sites, so the species PX_2Y may be formed at finite concentrations within experimental reach. Column A of Figure 7 describes the situation in which Y binds independently to a protein that has already bound 2 mol of X with homotropic positive cooperativity. Since the binding of X and the binding of Y are not energetically coupled in this scenario, Y may bind in any order without influencing the magnitude of the individual changes in free energy for the binding of either equivalent of X. Columns B−D describe the three possible orders of ligand addition where the following three conditions apply: (i) X and Y oppose each other's binding to spatially distinct sites on the antibody, (ii) the binding of 2 mol of X occurs with homotropic positive cooperativity in the absence of bound Y, and (iii) the binding of 2 mol of X occurs in a homogeneous fashion when Y is bound to the protein. It should be noted from columns C and D that the same intermediate product, PXY, is formed as the result of two successive binding equilibria where either X binds first followed by Y or Y binds first followed by X. When the principle of the conservation of free energy is applied to the stepwise formation of the biliganded species PXY as depicted in columns C and D, it is evident that

$$\Delta G(\mathrm{X}) + \Delta G(\mathrm{Y/X}) = \Delta G(\mathrm{Y}) + \Delta G(\mathrm{X/Y}) \quad (6)$$

Equation 6 reflects the reciprocal nature of the negative interaction between X and Y; that is, the prior binding of X has the same effect on the subsequent binding of Y as does the prior binding of Y on the subsequent binding of X. Similarly, it may be seen that

$$\Delta G(\mathrm{X/X}) + \Delta G(\mathrm{Y/X_2}) = \Delta G(\mathrm{Y/X}) + \Delta G(\mathrm{X/XY}) \quad (7)$$

In this case where X and Y oppose each other's binding, the coupling free energy change, $\Delta G_{2X,Y}$, will have a positive value given by

$$\Delta G_{2\mathrm{X,Y}} = \Delta G(\mathrm{Y}) - \Delta G(\mathrm{Y/X_2}) \quad (8)$$

where eq 8 is one of five combinations of free energy changes that could yield the same value of $\Delta G_{2X,Y}$. Equations 6−8 and the definition of $\Delta G_{X,X}$ (introduced above and in Table 2) lower the degrees of freedom in the thermodynamic cycles represented by the binding reactions in columns B−D of Figure 7 such that only five of the nine individual free energy changes must be independently determined to completely describe the entire set of linked equilibria.

Figure 8A presents equilibrium data for the binding of DCP−UO_2^{2+} to the 8A11−Cy5 covalent conjugate determined in the presence of five different concentrations of protein G. Since the abscissa uses a logarithmic scale to facilitate the presentation of a wide range of protein G concentrations, equilibrium binding data obtained with DCP−UO_2^{2+} and 8A11−Cy5 in the absence of protein G are not represented. When the principles of mass action and the conservation of free energy are applied to the binding schemes depicted in columns B−D of Figure 7 (*24*), the saturation function for X is as follows:

$$\begin{aligned}\text{fraction of sites occupied with X} = \{&[\mathrm{X}]/[K(\mathrm{X})] + [\mathrm{X}]^2/\\ &[K(\mathrm{X})K(\mathrm{X/X})] + ([\mathrm{X}][\mathrm{Y}])/[K(\mathrm{Y})K(\mathrm{X/Y})] + ([\mathrm{X}]^2[\mathrm{Y}])/\\ &[K(\mathrm{X/XY})K(\mathrm{X/Y})K(\mathrm{Y})]\}/\{1 + (2[\mathrm{X}])/[K(\mathrm{X})] + [\mathrm{X}]^2/\\ &[K(\mathrm{X})K(\mathrm{X/X})] + [\mathrm{Y}]/[K(\mathrm{Y})] + (2[\mathrm{X}][\mathrm{Y}])/\\ &[K(\mathrm{Y})K(\mathrm{X/Y})] + ([\mathrm{X}]^2[\mathrm{Y}])/[K(\mathrm{X/XY})K(\mathrm{X/Y})K(\mathrm{Y})]\} \quad (9)\end{aligned}$$

where $K(\mathrm{X})$ and $K(\mathrm{X/X})$ are as defined for eq 5, $K(\mathrm{Y}) = ([\mathrm{P}][\mathrm{Y}])/[\mathrm{PY}]$, $K(\mathrm{X/Y}) = ([\mathrm{PY}][\mathrm{X}])/[\mathrm{PXY}]$, and $K(\mathrm{X/XY}) = ([\mathrm{PXY}][\mathrm{X}])/[\mathrm{PX_2Y}]$. Values for all five equilibrium dissociation constants represented in eq 9 were obtained from a nonlinear regression fit of eq 9 to the data in Figure 8A. The parameters for the network of curves drawn through the data points in Figure 8A were determined from the nonlinear regression fit.

The ability of eq 9 to accurately describe the equilibrium binding data plotted in Figure 8A was ascertained by inspection of the residual plot shown in Figure 8B. Figure 8B shows the differences among the actual experimental data and the theoretical curve calculated using eq 9 and the values for the equilibrium constants obtained from the fit. The majority (>80%) of the experimental data in Figure 8B was within ±3% of the corresponding calculated value. The random dispersion of the experimental data above and below the theoretical plane was taken as evidence that eq 9

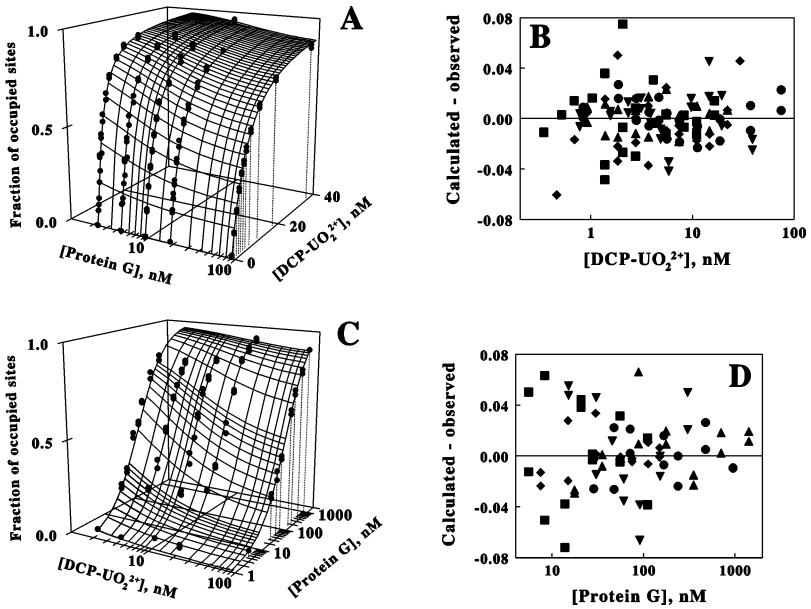

FIGURE 8: Heterotropic negative cooperativity in the binding of DCP−UO_2^{2+} and protein G to the 8A11−Cy5 covalent conjugate. (A) Equilibrium binding of DCP−UO_2^{2+} to 8A11−Cy5 in the presence of 2.3, 4.6, 9.2, 18.4, and 92 nM protein G. The parameters for the three-dimensional contour drawn through the data points were generated from a nonlinear regression global fit of the entire data set to eq 9. (B) Residual plot, showing the differences among the experimental data from panel A and the theoretical data using eq 9. The circles, triangles, squares, inverted triangles, and diamonds represent protein G concentrations of 2.3, 4.6, 9.2, 18.4, and 92 nM, respectively. (C) Equilibrium binding of protein G to 8A11−Cy5 in the presence of 2.3, 4.6, 9.2, 18.4, and 92 nM DCP−UO_2^{2+}. The parameters for the three-dimensional contour drawn through the data points were generated from a nonlinear regression global fit of the entire data set to eq 10. (D) Residual plot, showing the differences among the experimental data from panel C and the theoretical data using eq 10. The circles, triangles, squares, inverted triangles, and diamonds represent DCP−UO_2^{2+} concentrations of 2.3, 4.6, 9.2, 18.4, and 92 nM, respectively.

Table 4: Individual Free Energy Changes for the Coupled Binding of 2 mol of DCP−UO_2^{2+} and 1 mol of Protein G to the 8A11−Cy5 Covalent Conjugate

free energy change	observed value (kcal/mol)
unconditional	
ΔG(DCP−UO_2^{2+})	−11.4
ΔG(protein G)	−11.3
conditional	
ΔG(DCP−UO_2^{2+}/DCP−UO_2^{2+})	−12.9
ΔG(DCP−UO_2^{2+}/protein G)	−11.2
ΔG(DCP−UO_2^{2+}/DCP−UO_2^{2+},protein G)	−11.2
ΔG (proteinG/2DCP−UO_2^{2+})	−9.4
ΔG(protein G/DCP−UO_2^{2+})	−11.1
coupling	
$\Delta G_{\text{DCP}-UO_2^{2+},\text{DCP}-UO_2^{2+}}$	−1.5
$\Delta G_{\text{protein G,2DCP}-UO_2^{2+}}$	1.9

constituted an acceptable model for the binding of DCP−UO_2^{2+} to 8A11−Cy5 in the presence of protein G.

When converted to the corresponding free energy changes, the values for the five equilibrium constants obtained from the fit of eq 9 to the data in Figure 8A yielded values for ΔG(X), ΔG(X/X), ΔG(Y), ΔG(X/Y), and ΔG(X/XY). The values of ΔG(Y/X) and ΔG(Y/X_2) were obtained by substituting the five experimentally determined values into eqs 6 and 7, respectively. The remaining value of $\Delta G_{2X,Y}$ was then obtained using eq 8, while the value of $\Delta G_{X,X}$ was calculated as described above. The values of all nine free energy changes determined as described herein are summarized in Table 4. These nine values are necessary and sufficient for providing a complete thermodynamic description of the binding data presented in Figure 8A.

Figure 8C presents equilibrium data for the binding of protein G to the 8A11−Cy5 covalent conjugate determined in the presence of five different concentrations of DCP−UO_2^{2+}. Equilibrium binding data obtained with protein G and 8A11−Cy5 in the absence of DCP−UO_2^{2+} are not represented. Once again, when the principles of mass action and the conservation of free energy are applied to the binding schemes depicted in columns B−D of Figure 7, the saturation function for Y is as follows:

$$\text{fraction of sites occupied with Y} = \{[Y]/[K(Y)] + (2[X][Y])/[K(Y)K(X/Y)] + ([X]^2[Y])/[K(X)K(X/X)K(Y/X_2)]\}/\{1 + (2[X])/[K(X)] + [X]^2/[K(X)K(X/X)] + [Y]/[K(Y)] + (2[X][Y])/[K(X)K(Y/X)] + ([X]^2[Y])/[K(X)K(X/X)K(Y/X_2)]\} \quad (10)$$

where K(Y/X) = ([PX][Y])/[PXY], K(Y/X_2) = ([PX_2][Y])/[PX_2Y], and the other three equilibrium dissociation constants are as defined in eq 9. Values for the five equilibrium dissociation constants represented in eq 10 were obtained from a nonlinear regression fit of eq 10 to the data in Figure 8C. The parameters for the network of curves drawn through the data points in Figure 8C were determined from the nonlinear regression fit.

The ability of eq 10 to accurately describe the equilibrium binding data plotted in Figure 8C was ascertained by inspection of the residual plot shown in Figure 8D. Figure 8D shows the differences among the actual experimental data and the theoretical curve calculated using eq 10 and the values for the equilibrium constants obtained from the fit. The majority (>80%) of the experimental data in Figure 8D was within ±4% of the corresponding calculated value. The random dispersion of the experimental data above and below the theoretical plane was taken as evidence that eq 10

constituted an acceptable model for the binding of protein G to 8A11−Cy5 in the presence of DCP−UO_2^{2+}.

When converted to the corresponding free energy changes, the values for the five equilibrium constants obtained from the fit of eq 10 to the data in Figure 8C yielded values for ΔG(X), ΔG(X/X), ΔG(Y), ΔG(Y/X), and ΔG(Y/X_2). The values of ΔG(X/Y), ΔG(X/XY), and $\Delta G_{2X,Y}$ were obtained by substituting the five experimentally determined values into eqs 6−8, respectively. The values of these eight free energy changes calculated from the data in Figure 8C were identical, within experimental error, to those reported in Table 4. It is satisfactory, if not extraordinary, that the complex behavior reported in panels A and C of Figure 8 can be rationalized with the relatively simple three-site energetic binding model presented in Figure 7.

DISCUSSION

The observation that covalent modification of 8A11 with the *N*-hydroxysuccinimidyl ester of Cy5 stimulated its binding affinity for all seven antigen congeners while the analogous modification of the antibody with the succinimidyl ester of Alexa 488 carboxylic acid did not is not without precedent. Martsev et al. (*26*) described the covalent modification of a monoclonal antibody directed against human spleen ferritin with the carbodiimide-activated carboxylic acid and the *N*-hydroxysuccinimidyl ester of palladium(II) coproporphyrin I. Covalent modification of the antibody with the former reagent inhibited its antigen binding activity, while modification with the latter served to stimulate the affinity of the antibody for ferritin by 3-fold. Similarly, Ueno et al. reported a 4- and 8-fold stimulation of the affinities for monoclonal antibodies directed against BSA and the human c-erbB-2 protooncogene product, respectively, upon covalent modification of the antibodies with sulfosuccinimidyl nitrobenzamido derivatives (*27*).

The unprecedented feature of the covalent activation of 8A11 reported herein is the observation that the covalently modified antibody exhibited homotropic positive cooperativity in its antigen binding behavior, a property not observed with the unmodified protein. Even this observation can be rationalized if one considers that 8A11, like all antibodies, is a protein. Individual proteins can exhibit a wide variety of allosteric binding phenomena in the presence of appropriate binding partners and solution conditions. In principle, individual antibodies like chemically modified 8A11 could exhibit the same wide variety of allosteric phenomena. It is generally accepted that proteins maintain secondary, tertiary, and quaternary structure by virtue of a large number of independent, or nearly independent, short-range, small energy interactions. When an antigen is bound by an antibody, groups in the antigen and the antibody participate in new short-range weak interactions that comprise the binding interaction. Consequently, certain points along the peptide chain that forms the antigen binding site are now subject to forces not present in the absence of the antigen. That is, the addition of bound antigen must always produce some changes in the energetic balance of its immediate surroundings at the antibody binding site. Given the continuity of the covalently bonded peptide chain and the compact character of its folding, the effects of these bound antigen-induced forces may be transmitted and felt at many points in the antibody's structure. Not surprisingly, detailed structural studies on Fab fragments directed toward a variety of antigens have confirmed that significant conformation changes can occur within the Fab as a consequence of antigen binding.

X-ray crystallographic studies conducted on Fab fragments have clearly shown that certain antibodies undergo significant conformation changes throughout the structure of the Fab when the antigen binds (*28*−*33*). Thus, the Fab fragments derived from antibodies designated as 50.1 (directed against an HIV-1 peptide), NC6.8 (an N,N′,N‴-trisubstituted guanidine artificial sweetner), 13B5 (HIV-1 capsid protein p24), and OPG2 (peptide from the β3 subunit of integrin) were each reported to undergo substantial rearrangements in the third complementarity region of the heavy chain upon antigen binding. In addition, antigen binding produced changes in the relative rotation of the heavy and light chain variable regions of 8°, 15°, and 31° for the Fab fragments of antibodies 13B5, OPG2, and NC6.8, respectively. Notably, antigen binding-dependent conformation changes in the carboxyl domains far removed from the variable regions were reported for the Fab fragments of both OPG2 and NC6.8. Other reports using intact monoclonal antibodies directed against fluorescein and lysozyme have revealed that secondary interactions external to the antibody active site can affect antigen binding efficiency, protein dynamics, and variable domain conformation (*34*−*40*). While none of these intact antibodies has been reported to exhibit allosteric binding of its respective antigens, these structural studies do provide a mechanistic foundation for the speculation that allosteric binding behavior could be observed in individual antibodies under the right conditions. All that would be required is that conformation changes attendant with antigen binding at one of the two sites on the antibody result in a different conformation at the other, unoccupied antigen binding site.

Given the argument advanced above, there is no a prioi reason to presume that antigen binding-dependent conformation changes at one antigen binding site are necessarily limited to influences at the other antigen binding site; the constant regions of an individual antibody could be influenced by antigen binding as well. Indeed, there are both older spectroscopic (*41*, *42*) and more recent direct binding studies (*43*, *44*) that provide evidence of allosteric conformation changes in the antibody's constant regions upon antigen binding. The latter studies described the protein A binding properties of two different monoclonal antibodies (G10 and F11) directed against human ferritin. Protein A, like protein G, is a bacterial cell wall protein that binds to the constant region of certain mouse immunoglobulins. When ferritin bound to antibodies G10 and F11, the affinities of the antibodies for protein A increased and decreased, respectively, relative to the affinities exhibited for protein A in the absence of ferritin. Similarly, the binding of 4-hydroxy-3-nitrophenyl-ϵ-aminocaproic acid (NP-Cap) to mouse antibodies directed against NP-Cap served to lower the affinity of the antibodies for either protein A or protein G (*44*). The same laboratory had shown much earlier that C1q, the first component of complement that binds to the CH_2 constant region of mouse heavy chains, bound to an anti-NP-Cap monoclonal antibody and increased its affinity for the antigen (*45*). The binding experiments described herein with 8A11−Cy5, protein G, and the Zenon Fab fragments provide the

most complete description to date of the energetics of the effects of multiple ligand interactions on the binding behavior of the variable and constant regions of an antibody.

That noncovalent modification of an antibody in its constant region could alter the affinity of the antibody for its antigen could have widespread implications in the practical applications or fundamental studies of such antibodies. The number or frequency of occurrence of antibodies that exhibit changes in their antigen binding properties when selected ligands bind to distant sites on the Fc portion of the protein is not known. The fact that 8A11 and other antibodies appear to do so implies that, in principle, any antibody could display some aspect of the behavior summarized herein. It would be of interest to investigate whether binding of the natural Fc receptor to selected monoclonal antibodies would serve to influence the affinity of the bound antibody for its antigen. It is anticipated that further studies will contribute to a basic understanding of a heretofore poorly characterized aspect of antibody function.

On a practical level, the purposeful manipulation of allosteric binding behavior could extend the clinical and therapeutic applications of antibodies. Diagnostic immunochemical assays may be arbitrarily divided into two major categories: those that quantify an analyte within a given concentration range and those that identify the presence of an analyte above a given threshold concentration. In the latter assays, an antibody that exhibited homotropic positive cooperativity with the steep portion of the sigmoidal binding curve just below the given threshold concentration would likely be a superior reagent for answering a simple "yes" or "no" diagnostic question.

SUPPORTING INFORMATION AVAILABLE

Two tables (1S and 2S) of equilibrium dissociation constants for the binding of metal-free chelators to chemically modified 8A11 and its proteolytic fragments. This material is available free of charge via the Internet at http://pubs.acs.org.

REFERENCES

1. Blake, R. C., II, Delehanty, J. B., Khosraviani, M., Yu, H., Jones, R. M., and Blake, D. A. (2003) Allosteric binding properties of a monoclonal antibody and its Fab fragment, *Biochemistry 42*, 497−508.
2. Reardan, D. T., Meares, C. F., Goodwin, D. A., McTigue, M., David, G. S., Stone, M. R., Leung, J. P., Bartholomew, R. M., and Frincke, J. M. (1985) Antibodies against metal chelates, *Nature 316*, 265−268.
3. Love, R. A., Villafranca, J. E., Aust, R. M., Nakamura, K. K., Jue, R. A., Major, J. G., Jr., Radhakrishnan, R., and Butler, W. F. (1993) How the anti-(metal chelate) antibody CHA255 is specific for the metal ion of its antigen: X-ray structures for two Fab′/hapten complexes with different metals in the chelate, *Biochemistry 32*, 10950−10959.
4. Boden, V., Colin, C., Barbet, J., Le Doussal, J. M., and Vijayalakshmi, M. (1995) Preliminary study of the metal binding site of an anti-DTPA-indium antibody by equilibrium binding immunoassays and immobilized metal ion affinity chromatography, *Bioconjugate Chem. 6*, 373−379.
5. Blake, D. A., Chakrabarti, P., Khosraviani, M., Hatcher, F. M., Westhoff, C. M., Goebel, P., Wylie, D. E., and Blake, R. C., II (1996) Metal binding properties of a monoclonal antibody directed towards metal-chelate complexes, *J. Biol. Chem. 271*, 27677−27685.
6. Blake, D. A., Blake, R. C., II, Khosraviani, M., and Pavlov, A. R. (1998) Metal ion immunoassays, *Anal. Chim. Acta 376*, 13−19.
7. Feng, X., Pak, R. H., Kroger, L. A., Moran, J. K., DeNardo, D. G., Meares, C. F., DeNardo, G. L., and DeNardo, S. J. (1998) New anti-Cu-TETA and anti-Y-DOTA monoclonal antibodies for potential use in the pre-targeted delivery of radiopharmaceuticals to tumors, *Hybridoma 17*, 125−132.
8. Westhoff, C. M., Lopez, O., Goebel, P., Carlson, L., Carlson, R. R., Wagner, F. W., Schuster, S. M., and Wylie, D. E. (1999) Unusual amino acid usage in the variable regions of mercury-binding antibodies, *Proteins 37*, 429−440.
9. DeNardo, S. J., DeNardo, G. L., Brush, J., and Carter, P. (1999) Phage library-derived human anti-TETA and anti-DOTA ScFv for pretargeting RIT, *Hybridoma 18*, 13−21.
10. Khosraviani, M., Blake, R. C., II, Pavlov, A. R., Lorbach, S. C., Yu, H., Delehanty, J. B., Brechbiel, M. W., and Blake, D. A. (2000) Binding properties of a monoclonal antibody directed toward lead-chelate complexes, *Bioconjugate Chem. 11*, 267−277.
11. Blake, D. A., Pavlov, A. R., Yu, H., Khosraviani, M., Ensley, H. E., and Blake, R. C., II (2001) Antibodies and antibody-based assays for hexavalent uranium, *Anal. Chim. Acta 444*, 3−11.
12. Jones, R. M., Yu, H., Delehanty, J. B., and Blake, D. A. (2002) Monoclonal antibodies that recognize minimal differences in the 3-dimensional structures of metal-chelate complexes, *Bioconjugate Chem. 13*, 408−415.
13. Delehanty, J. B., Jones, R. M., Bishop, T. C., and Blake, D. A. (2003) Identification of important residues in metal-chelate recognition by monoclonal antibodies, *Biochemistry 42*, 14173−14183.
14. Corneillie, T. M., Whetstone, P. A., Fisher, A. J., and Meares, C. F. (2003) A rare earth-DOTA-binding antibody: Probe properties and binding affinity across the lanthanide series, *J. Am. Chem. Soc. 125*, 3436−3437.
15. Blake, R. C., II, Pavlov, A. R., Khosraviani, M., Ensley, H. E., Keifer, G. E., Yu, H., Li, X., and Blake, D. A. (2004) Novel monoclonal antibodies with specificity for chelated uranium(VI): Isolation and binding properties, *Bioconjugate Chem. 15*, 1125−1136.
16. Sumner, M. T. (1993) Association constants of anti-hapten monoclonal IgG1 with mouse FcγRII in the presence and absence of hapten, *FEBS Lett. 333*, 35−38.
17. Baird, C. L., and Myszka, D. G. (2001) Current and emerging commercial optical biosensors, *J. Mol. Recognit. 14*, 261−268.
18. Squillante, E., III (1998) Applications of fiber-optic evanescent wave spectroscopy, *Drug Dev. Ind. Pharm. 24*, 1163−1175.
19. Smith, R. H., Lemon, W. J., Erb, J. L., Erb-Downward, J. R., Downward, J. G., Ulrich, O. E., and Wittliff, J. L. (1999) Development of kinetic ligand-binding assays using a fiber optic sensor, *Clin. Chem. 45*, 1683−1685.
20. Blake, R. C., II, Pavlov, A. R., and Blake, D. A. (1999) Automated kinetic exclusion assays to quantify protein binding interactions in homogeneous solution, *Anal. Biochem. 272*, 123−134.
21. Blake, R. C., II, and Blake, D. A. (2004) Kinetic exclusion assay to study high-affinity binding interactions in homogeneous solutions, *Methods Mol. Biol. 248*, 417−430.
22. Weber, G. (1975) Energetics of ligand binding to proteins, *Adv. Protein Chem. 29*, 1−83.
23. Weber, G. (1972) Ligand binding and internal equilibria in proteins, *Biochemistry 11*, 864−878.
24. Weber, G. (1965) The binding of small molecules to proteins, in *Molecular Biophysics* (Pullman, B., and Weissbluth, M., Eds.) pp 369−396, Academic Press, New York.
25. Sauer-Eriksson, A. E., Kleywegt, G. J., Uhlen, M., and Jones, T. A. (1995) Crystal structure of the C2 fragment of streptococcal protein G in complex with the Fc domain of human IgG, *Structure 3*, 265−278.
26. Martsev, S. P., Preygerzon, V. A., Melnikova, Y. I., Kravchuk, Z. I., Ponomarv, G. V., Lunev, V. E., and Savisky, A. P. (1995) Modification of monoclonal and polyclonal IgG with palladium-(II) coproporphyrin I: Stimulatory and inhibitory functional effects induced by two different methods, *J. Immunol. Methods 186*, 293−304.
27. Ueno, H., Masuko, T., Wang, J., and Hashimoto, Y. (1993) Enhanced binding to antigen of monoclonal antibodies modified with a crosslinker, *Biochem. Biophys. Res. Commun. 191*, 701−708.
28. Guddat, L. W., Shan, L., Anchin, J. M., Linthicum, D. S., and Edmundson, A. B. (1994) Local and transmitted conformational changes on complexation of an anti-sweetener Fab, *J. Mol. Biol. 236*, 247−274.

29. Stanfield, R. L., Takimoto-Kamimura, M., Rini, J. M., Profy, A. T., and Wilson, I. A. (1993) Major antigen-induced domain rearrangements in an antibody, *Structure 1*, 83−93.
30. Kodandapani, R., Veerapandian, L., Ni, C. Z., Chiou, C. K., Whittal, R. M., Kunicki, T. J., and Ely, K. R. (1998) Conformational change in an anti-integrin antibody: Structure of OPG2 Fab bound to a β3 peptide, *Biochem. Biophys. Res. Commun. 251*, 61−66.
31. Monaco-Malbet, S., Berthet-Colominas, C., Novelli, A., Battai, N., Piga, N., Cheynet, V., Mallet, F., and Cusack, S. (2000) Mutual conformational adaptations in antigen and antibody upon complex formation between an Fab and HIV-1 capsid protein p24, *Structure 8*, 1069−1077.
32. Rini, J. M., Schulze-Gahmen, U., and Wilson, I. A. (1992) Structural evidence for induced fit as a mechanism for antibody-antigen recognition, *Science 255*, 959−965.
33. Herron, J. N., He, X. M., Blier, P. R., Pace, P. E., Bothwell, A. L., Voss, E. W., Jr., and Edmundson, A. B. (1991) An autoantibody to single-stranded DNA: Comparison of the three-dimensional structures of the unliganded Fab and a deoxynucleotide-Fab complex, *Proteins 11*, 159−175.
34. Mummert, M. E., and Voss, E. W., Jr. (1996) Effects of secondary forces on the ligand binding properties and variable domain conformations of a monoclonal anti-fluorescyl antibody, *Mol. Immunol. 33*, 1067−1077.
35. Mummert, M. E., and Voss, E. W., Jr. (1997) Effects of secondary forces on the ligand binding and conformation state of antifluorescein monoclonal antibody 9-40, *Biochemistry 36*, 11918−11922.
36. Mummert, M. E., and Voss, E. W., Jr. (1996) Effects of secondary forces on a high affinity monoclonal IgM anti-fluorescein antibody possessing cryoglobulin and other cross-reactive properties, *Mol. Immunol. 35*, 103−113.
37. Mummert, M. E., and Voss, E. W., Jr. (1996) Secondary force-mediated perturbations of antifluorescein monoclonal antibodies 4-4-20 and 9-40 as determined by circular dichroism, *J. Protein Chem. 17*, 237−244.
38. Benjamin, D. C., Williams, D. C., Jr., Smith-Gill, S. J., and Rule, G. S. (1992) Long-range changes in a protein antigen due to antigen-antibody interaction, *Biochemistry 31*, 9539−9545.
39. Lavoie, T. B., Drohan, W. N., and Smith-Gill, S. J. (1992) Experimental analysis by site-directed mutagenesis of somatic mutation effects on affinity and fine specificity in antibodies specific for lysozyme, *J. Immunol. 148*, 503−513.
40. Padlan, E. A., Silverton, E. W., Sheriff, S., Cohen, G. H., Smith-Gill, S. J., and Davies, D. R. (1989) Structure of an antibody-antigen complex: Crystal structure of the HyHEL-10 Fab-lysozyme complex, *Proc. Natl. Acad. Sci. U.S.A. 86*, 5938−5942.
41. Jaton, J. C., Huser, H., Braun, D. G., Givol, D., Pecht, I., and Schlessinger, J. (1975) Conformational changes induced in a homogeneous anti-type III pneumococcal antibody by oligosaccharides of increasing size, *Biochemistry 14*, 5312−5315.
42. Schlessinger, J., Steinberg, I. Z., Givol, D., Hochman, J., and Pecht, I. (1975) Antigen-induced conformational changes in antibodies and their Fab fragments studied by circular polarization of fluorescence, *Proc. Natl. Acad. Sci. U.S.A. 72*, 2775−2779.
43. Kravchuk, Z. I., Chumanevich, A. A., Vlasov, A. P., and Martsev, A. P. (1998) Two high-affinity monoclonal IgG2a antibodies with differing thermodynamic stability demonstrate distinct antigen-induced changes in protein A-binding affinity, *J. Immunol. Methods 217*, 131−141.
44. Oda, M., Kozono, H., Morii, H., and Azuma, T. (2003) Evidence of allosteric conformational changes in the antibody constant region upon antigen binding, *Int. Immunol. 15*, 417−426.
45. Hamada, A., Watanabe, N., Azuma, T., and Kobayashi, A. (1990) Enhancing effect of C1q on IgG monoclonal antibody binding to hapten, *Int. Arch. Allergy Appl. Immunol. 91*, 103−107.

BI062164J